ACS OMEGA

Open Access

This article is licensed under CC-BY-NC-ND 4.0

http://pubs.acs.org/journal/acsodf

Article

A Facile and Biocompatible Hydrogel Based on Oxidized *Brachybotrys paridiformis* Polysaccharide for Enhanced Wound Healing

Na Zou,[§] Jie Zhou,[§] Xifan Mei,* Qing Chen,* and Sitong Wu*

Cite This: *ACS Omega* 2026, 11, 20646−20656

Read Online

ACCESS | Metrics & More | Article Recommendations | Supporting Information

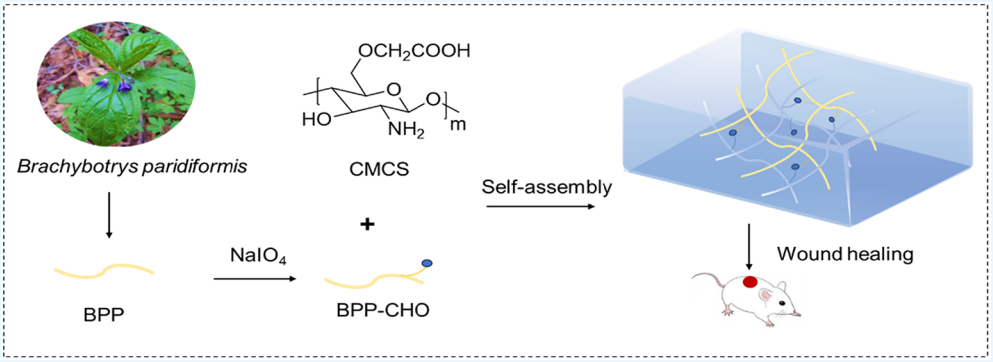

ABSTRACT: *Brachybotrys paridiformis* polysaccharide (BPP) was extracted from the edible plant *B. paridiformis*, and its extraction conditions were systematically optimized using single-factor experiments combined with response surface methodology. Building upon the extracted BPP, an innovative hydrogel wound dressing was fabricated via a Schiff base reaction between oxidized BPP (OBPP) and *O*-carboxymethyl chitosan (CMCS). The resulting OBPP/CMCS hydrogel displayed a highly interconnected porous architecture and desirable swelling characteristics, along with excellent biocompatibility and the ability to promote human umbilical vein endothelial cells (HUVECs) migration in vitro. In vivo studies demonstrated the hydrogel's outstanding wound-healing performance, characterized by accelerated wound closure and scar-suppressed tissue regeneration. By day 9, the hydrogel-treated group showed a significantly smaller wound area (7.59 ± 1.83%) compared with the control group (44.14 ± 18.22%). By day 15, the hydrogel group achieved nearly complete healing, featuring smooth, scab-free skin, in contrast to the incomplete recovery observed in other groups. These findings underscore the hydrogel's strong potential as an effective and multifunctional wound dressing.

1. INTRODUCTION

The skin functions as the body's foremost defense barrier, protecting internal tissues from external harm. In everyday life, injuries such as surgical incisions, abrasions, cuts, and burns occur frequently.[1,2] Although the skin naturally heals itself, appropriate wound management remains essential to minimize bleeding, prevent infection, relieve discomfort, and accelerate proper tissue repair.[3,4] Traditional dressings like gauze, however, suffer from certain drawbacks, including strong adhesion to the wound surface and poor moisture retention. These limitations have led to the emergence of advanced wound care materials such as hydrogels, hydrocolloids, and semipermeable foams. Among these, hydrogel dressings have gained prominence for their ability to maintain an ideal moist environment and promote tissue regeneration.[5,6]

Hydrogels represent a distinct class of polymeric materials characterized by their hydrophilic, three-dimensional network structures.[7] Owing to these interconnected hydrophilic matrices, hydrogels can effectively retain moisture at the wound site, an essential condition for promoting cellular migration and facilitating autolytic debridement.[8,9] Beyond their basic wound-healing properties, hydrogels have evolved into highly adaptable platforms for a broad spectrum of biomedical applications. Examples include thermoresponsive systems for controlled drug delivery,[10] supramolecular assemblies for localized cancer therapy,[11] and three-dimensional tumor models for drug screening.[12] Nevertheless, many hydrogels still rely on organic cross-linkers such as glutaraldehyde, raising biosafety concerns, while their passive nature limits dynamic regulation of the wound microenvironment.[5] In this context, natural polysaccharides have emerged as ideal structural

Received: November 26, 2025
Revised: March 24, 2026
Accepted: March 25, 2026
Published: March 28, 2026

© 2026 The Authors. Published by American Chemical Society

components due to their intrinsic biodegradability, excellent biocompatibility, and diverse bioactivities. Their inherent antioxidant and anti-inflammatory properties further improve the healing process, making them particularly valuable in the design of next-generation wound dressings.[13−16] In this paper, *Brachybotrys paridiformis* Maxim. ex Oliv. was studied, a perennial plant valued as a wild vegetable resource and widely grown in Korea, Russia, and Northeast China.[17] Although lignans and phenylpropanoids with anti-inflammatory and anti-HBV activities have been reported,[18−20] the polysaccharide of *B. paridiformis* (BPP) remains unexplored, and its potential application in biomedical fields such as wound healing has not been reported. The strategy was to transform BPP from a bioactive extract into the core structural and functional scaffold of a hydrogel network. This was achieved by assessing its bioactivity and constructing a natural hydrogel through the cross-linking of OBPP with CMCS, thereby circumventing the need for synthetic cross-linking agents.[21,22]

In this study, an optimized extraction method for BPP and the subsequent fabrication of an OBPP/CMCS hydrogel were successfully developed. The hydrogel dressing exhibited desirable physicochemical characteristics, including a well-defined porous microstructure and exceptional swelling capacity. Furthermore, it demonstrated excellent biocompatibility and enhanced in vitro migratory activity of HUVECs. In vivo assessments using a full-thickness excisional wound model confirmed the hydrogel's outstanding ability to accelerate wound closure and promote high-quality tissue regeneration with minimal scarring. These results demonstrate the strong potential of the OBPP/CMCS hydrogel as an effective and multifunctional dressing for acute wound management.

2. MATERIALS AND METHODS

2.1. Materials

The plant material (*B. paridiformis* Maxim. ex Oliv.) was collected in Acheng District, Harbin City, Heilongjiang Province, and authenticated by Professor Guangshu Wang (School of Pharmacy, Jilin University).

Key reagents used in this study included 1,1-diphenyl-2-picrylhydrazyl (DPPH), 2,2′-azino-*bis*(3-ethylbenzothiazoline-6-sulfonic acid) (ABTS), hydrogen peroxide, and glucose standard, all purchased from Shanghai Macklin Biochemical Technology Co., Ltd. (Shanghai, China). Dialysis membranes with molecular weight cut-offs of 3.5 kDa and 8-14 kDa were obtained from Beijing Biotopped Technology Co., Ltd. (Beijing, China) and Shanghai Yuanye Bio-Technology Co., Ltd. (Shanghai, China), respectively. Cell culture reagents, including penicillin/streptomycin, phosphate-buffered saline (PBS), and premium fetal bovine serum (FBS), were supplied by Beijing Labgic Technology Co., Ltd. (Beijing, China). The 0.05% trypsin digestion solution was purchased from Shanghai Biocytogen Reagent Co., Ltd. (Shanghai, China), while Dulbecco's Modified Eagle Medium (DMEM) was sourced from Wuhan Pricella Biotechnology Co., Ltd. (Wuhan, China). *O*-Carboxymethyl chitosan (MW: 240 kDa; degree of deacetylation >90%; degree of substitution: 90%) and sodium periodate were procured from Shanghai Rhawn Reagent Co., Ltd. (Shanghai, China). All other analytical-grade chemicals were supplied by Xilong Scientific Co., Ltd. (Shenzhen, China).

2.2. Extraction and Process Optimization of BPP

BPP was extracted using a hot-water extraction followed by ethanol precipitation. The extraction conditions were systematically optimized through single-factor experiments and further refined using a Box-Behnken design (BBD) to evaluate the influence of key process parameters (see Section S1, Supporting Information, for detailed experimental procedures).[23,24]

2.3. Assay for Antioxidant Activities of BPP

The in vitro antioxidant capacity of BPP was assessed by determining its scavenging activity against DPPH, hydroxyl, and ABTS free radicals, following previously reported methods with minor modifications.[25−27] Detailed assay procedures and calculation methods are provided in Section S2 of the Supporting Information.

2.4. OBPP/CMCS Hydrogel Preparation

The oxidized polysaccharide (OBPP) was prepared following a modified sodium periodate oxidation protocol. Briefly, 1 g of BPP was dissolved in 100 mL of distilled water, followed by the addition of 0.7 g of sodium periodate. After the designated reaction time, the oxidation was terminated by adding 5 mL of ethylene glycol, and the mixture was stirred for another 2 h. The reaction solution was then dialyzed against deionized water for 72 h using a dialysis membrane with a molecular weight cutoff of 8-14 kDa, with the water replaced three times daily. The resulting product was subsequently lyophilized to yield OBPP.

For hydrogel fabrication, an aqueous OBPP solution (30% w/w) was combined with an equal volume of CMCS solution (20% w/w) to obtain a uniform mixture. The mixture was sonicated to eliminate entrapped air bubbles and subsequently allowed to gel at ambient temperature, resulting in the formation of the OBPP/CMCS hydrogel. Aldehyde content determination was carried out using the hydroxylamine hydrochloride titration method. Briefly, 100 mg of OBPP dried to constant weight was dissolved in 25 mL of 0.25 mol/L hydroxylamine hydrochloride solution, followed by the addition of two drops of bromophenol blue indicator. The mixture was titrated with 0.1 mol/L NaOH standard solution to a blue-purple end point. A blank titration was performed using 0.25 mol/L hydroxylamine hydrochloride solution without OBPP. All measurements were conducted in triplicate. In addition, to further verify the biosafety of the hydrogel system, residual free aldehyde groups in the hydrogel supernatant were also determined using the same method. The aldehyde content was calculated according to eq 1.[28]

$$\text{aldehyde content (mmol/g)} = \frac{(V_{\text{sample}} - V_{\text{blank}}) \times C_{\text{NaOH}}}{m} \quad (1)$$

where V_{sample} and V_{blank} are the titration volumes (mL) for the sample and blank, C_{NaOH} is the concentration of NaOH (0.1 mol/L), and m is the mass of OBPP (g).

2.5. Fourier Transform Infrared Analysis

Fourier transform infrared (FT-IR) was measured using the Nicolet 6700 FT-IR spectrometer (Thermo Fisher Scientific, USA) in the wavenumber range of 400−4000 cm^{-1} with a resolution of 4 cm^{-1} and 32 scans.

2.6. Rheology Analysis

The rheological behavior of the OBPP/CMCS hydrogel was analyzed using a rotational rheometer (MCR92, Anton Paar, Austria) at 37 °C. Strain sweep test was conducted from 1% to 500% at a fixed angular frequency of 10 rad·s^{-1} to determine the storage modulus (G') and loss modulus (G'') of the hydrogel. Frequency sweep test was performed from 1 to 100 rad·s^{-1} under a constant strain of 0.1% to evaluate the viscoelastic properties.

2.7. Swelling Performance and Moisture Retention of OBPP/CMCS Hydrogel

To evaluate the swelling behavior of the prepared hydrogel, preweighed hydrogel samples (W_i) were immersed in 5 mL of phosphate buffer (pH 5.5 and 7.4) and incubated at a constant temperature of 37 °C. At predetermined time intervals, the samples were removed, gently blotted to remove surface moisture, and weighed (W_a). This process was repeated until the difference between two consecutive measurements was less than 0.1 g. The swelling ratio was then calculated according to eq 2.[29]

$$\text{swelling ratio (\%)} = (W_a - W_i)/W_i \times 100\% \quad (2)$$

https://doi.org/10.1021/acsomega.5c12446
ACS Omega 2026, 11, 20646−20656

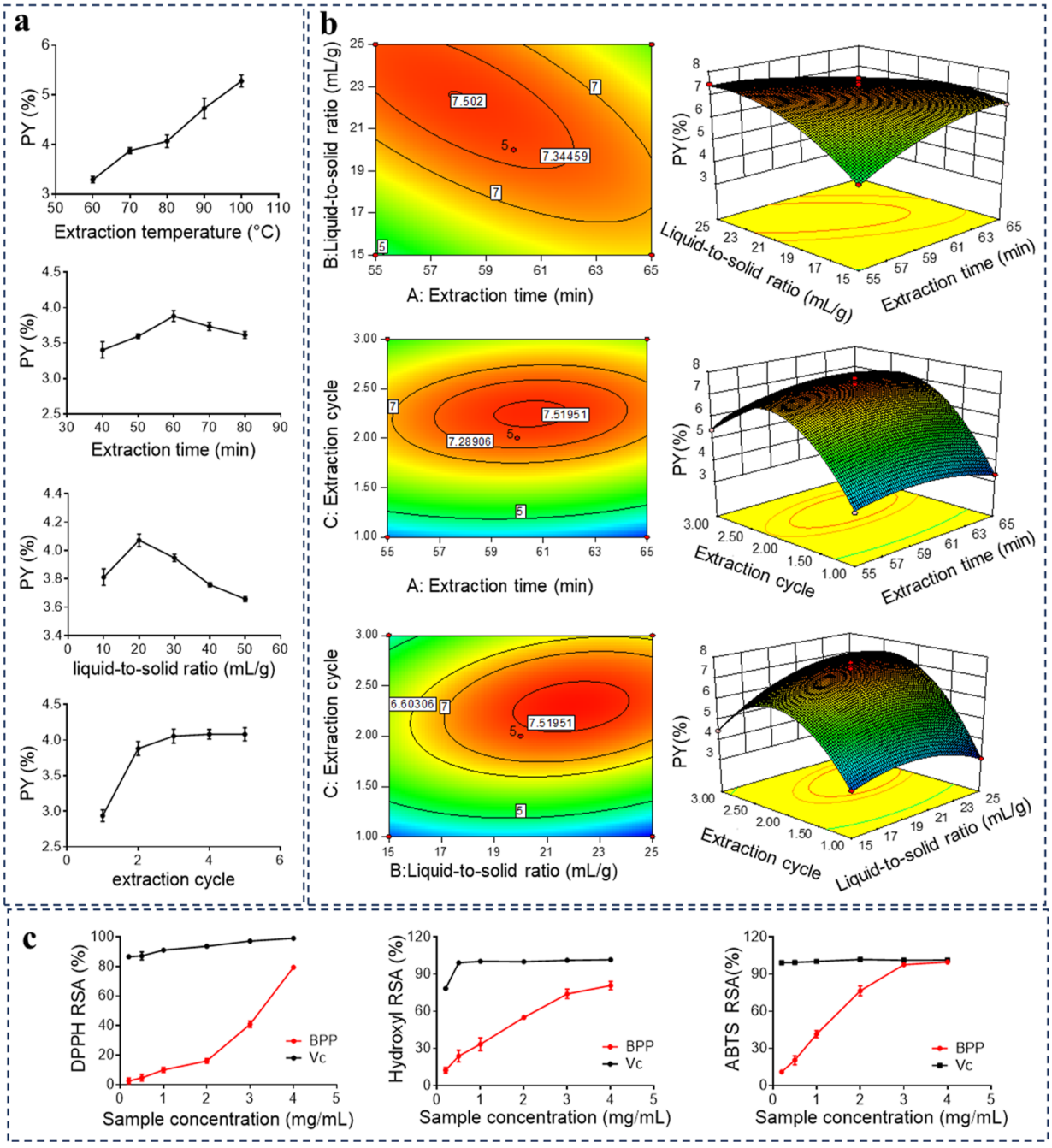

Figure 1. Extraction and Antioxidant Activity of BPP. (a) Effects of extraction parameters on the BPP yield (PY %; see Supporting Information S1.3 for detailed definition and calculation). Values are presented as means ± SD ($n = 3$). (b) The 3D response surface plots and contour plots of the influence of interactions on Polysaccharide yield. (c) Results of antioxidant assay of BPP.

After reaching swelling balance, the same swollen samples were kept in fresh PBS at 37 °C to test their long-term stability. At predetermined time intervals, samples were taken out, blotted dry, and weighed again (W_a). The weight kept at each time was compared to the weight at swelling equilibrium (W_0) using eq 3.[30]

$$\text{mass retention } (\%) = W_a/W_0 \times 100\% \quad (3)$$

To assess the water retention capacity, 1 g of the hydrogel was placed in an incubator at 37 °C for 12 h, and its initial weight was recorded as W_0. The weight of the sample (W_1) was measured at hourly intervals, and the water loss rate of the hydrogel was calculated using eq 4.

$$\text{water loss rate } (\%) = (W_0 - W_1)/W_0 \times 100\% \quad (4)$$

2.8. Scanning Electron Microscopy Analysis

The microstructural morphology of the lyophilized hydrogel was analyzed using scanning electron microscopy (SEM; Hitachi S4800, Japan). Briefly, the hydrogel samples were cryo-fractured, coated with a thin layer of gold, and imaged at an accelerating voltage of 3 kV. The average pore size was determined from the acquired micrographs using ImageJ software.

2.9. In Vitro Hemolysis Test of the Prepared Hydrogel

Fresh mouse blood was centrifuged at 1300 rpm for 10 min, and the supernatant was discarded. The obtained erythrocyte pellet was washed three to four times with physiological saline, and a 5% red blood cell suspension was prepared. The preformed hydrogel samples were first sterilized under ultraviolet (UV) light for 24 h. Subsequently, 0.04 g of

https://doi.org/10.1021/acsomega.5c12446
ACS Omega 2026, 11, 20646−20656

Table 1. ANOVA for the Response Surface Quadratic Model[a]

source	degree of freedom	sum of squares	mean square	F	P	sig
model	9	43.33	4.81	118.2	<0.0001	significant
extraction time (A)	1	0.014	0.014	0.33	0.5813	not significant
liquid−solid ratio (B)	1	1.22	1.22	30.07	0.0009	***
extraction cycle (C)	1	9.86	9.86	241.99	<0.0001	***
AB	1	2.98	2.98	73.05	<0.0001	***
AC	1	0.26	0.26	6.39	0.0394	*
BC	1	1.56	1.56	38.36	0.0004	***
A^2	1	1.04	1.04	25.46	0.0015	**
B^2	1	2.38	2.38	58.34	0.0001	***
C^2	1	22.35	22.35	548.62	<0.0001	***
residual	7	0.29	0.041			
lack of fit	3	0.035	0.012	0.18	0.9015	not significant
pure error	4	0.25				
cor total	16	43.62				

[a]*$p < 0.05$, **$p < 0.01$, ***$p < 0.001$.

the sterilized hydrogel was incubated with 2 mL of the erythrocyte suspension at 37 °C for 2 h. After incubation, the samples were centrifuged, and the hemoglobin content in the supernatant was measured at 540 nm to calculate the hemolysis ratio (HR %) according to eq 5.[31]

$$\mathrm{HR}\ (\%) = \frac{A_{\text{hydrogel sample}} - A_{\text{negative control}}}{A_{\text{positive control}} - A_{\text{negative control}}} \times 100\% \quad (5)$$

2.10. Cell Viability Test

The cytocompatibility of the hydrogel was further assessed using a CCK-8 assay on HUVECs. The sterilized hydrogel samples were extracted in culture medium at 37 °C for 24 h. HUVECs were seeded in 96-well plates at a density of 5×10^3 cells per well. After cell attachment, the culture medium was replaced with BPP or hydrogel extracts at concentrations of 50, 100, 200, 400, and 800 μg/mL, while the control group was maintained in fresh culture medium. Following 24 h of incubation, cell viability was evaluated using the CCK-8 assay, and absorbance was recorded at 450 nm with a FLUOstar Omega microplate reader (BMG LABTECH, Ortenberg, Germany). Cell viability was calculated using the following equation

$$\text{cell viability}\ (\%) = \frac{A_{\text{sample}} - A_{\text{blank}}}{A_{\text{control}} - A_{\text{blank}}} \times 100\% \quad (6)$$

where A_{sample} is the absorbance of cells treated with BPP or hydrogel extracts, A_{control} is the absorbance of untreated cells, and A_{blank} is the absorbance of the culture medium without cells.

2.11. Evaluation of Wound Healing In Vitro

HUVECs were seeded in 24-well plates at a density of 1×10^4 cells per well in 2 mL of culture medium. Upon reaching confluence, a linear scratch was introduced into the cell monolayer using a sterile 200 μL pipet tip, followed by two rinses with PBS to remove detached cells. The PBS was then replaced with either BPP solution or hydrogel extracts at concentrations of 200, 400, and 800 μg/mL, while the control group received only fresh culture medium. Images of the wound area were captured at 0, 24, and 48 h postscratch using an inverted microscope (AE2000, Motic, Xiamen, China), and the scratch areas at these time points were quantified with ImageJ.[32,33]

2.12. The Evaluation of Wound Healing In Vivo

Animals and Experimental Design:[34] After a two-day acclimatization period under standard laboratory conditions, Kunming mice (6−8 weeks of age, approximately 18−22 g, purchased from Liaoning Changsheng Biotechnology Co., Ltd. (Shenyang, China)) were randomly allocated into five groups (n = 5 per group): (1) negative control (wound treated with sterile gauze only), (2) 3 M group (treated with 3 M Cavilon No Sting Barrier Film, 3 M Health Care, Maplewood, MN, USA), (3) BPP group, (4) OBPP/CMCS hydrogel group, and (5) normal group (healthy mice without wound creation). Mice were anesthetized with 0.3% sodium pentobarbital (50 mg/kg), and the dorsal region was shaved. A full-thickness excisional wound (8 mm in diameter) was created on the back using sterile surgical scissors. The wounds in the control group were covered with sterile gauze, the positive control group received a commercial 3 M spray dressing, and the treatment groups were administered either the polysaccharide solution or a single layer of hydrogel. Treatments were applied topically once daily. Wound healing progression was recorded photographically on days 0, 3, 6, 9, 12, and 15, and the wound areas were quantified using ImageJ software. On day 15, wound tissues were excised, fixed in 4% paraformaldehyde for 24 h, embedded in paraffin, and sagittally sectioned into 4−5 μm slices. The sections were subsequently stained with hematoxylin and eosin (H & E) and examined under an inverted microscope for histological evaluation.

2.13. Statistical Analysis

Data analysis was performed using GraphPad Prism 10.4.0. All results are expressed as mean ± standard deviation (SD) based on at least three independent experiments (n = 3). One-way and two-way ANOVA with Tukey's test were used for statistical analysis, with significance levels indicated by asterisks: *$P < 0.05$, **$P < 0.01$, ***$P < 0.001$, and ****$P < 0.0001$.

3. RESULTS AND DISCUSSION

3.1. Effect of Process Parameters on the Yield of Polysaccharide

Figure 1a depicts the effects of different parameters on the extraction yield of BPP. A clear positive correlation was observed between temperature and extraction efficiency, with the maximum yield of (5.28 ± 0.12) % obtained at 100 °C, which was therefore selected as the optimal extraction temperature. The extraction yield peaked at 60 min, likely because shorter durations led to incomplete extraction, while prolonged heating promoted polysaccharide degradation, denaturation, or precipitation, lowering yield. Accordingly, an optimal extraction time range of 55−65 min was identified. Similarly, the yield reached its maximum at a liquid-to-solid ratio of 20:1 mL/g, aligning with previously reported findings;[35] thus, a range of 15:1−25:1 mL/g was adopted for further optimization. As the number of extraction cycles increased from one to two, the yield rose sharply from (2.98 ± 0.08) % to (3.88 ± 0.10) %, while a third cycle produced only a marginal improvement to (4.06 ± 0.10) %. Considering both efficiency and practicality, 1−3 extraction cycles were selected for subsequent response surface optimization.

https://doi.org/10.1021/acsomega.5c12446
ACS Omega 2026, 11, 20646−20656

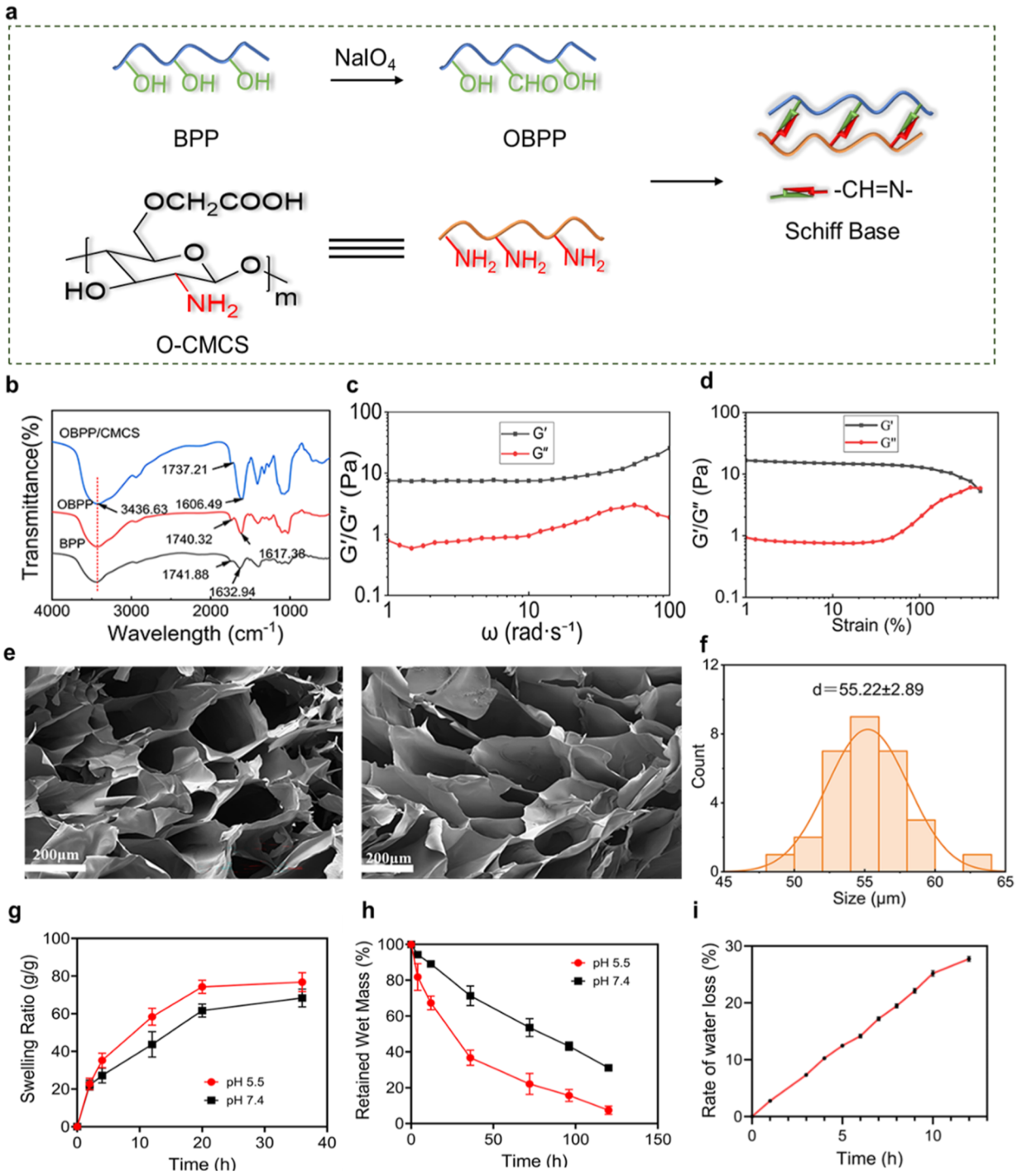

Figure 2. Synthesis of OBPP/CMCS and performance characterization of the OBPP/CMCS hydrogel. (a) Synthesis of the OBPP/CMCS hydrogel. Abbreviations: BPP, *Brachybotrys paridiformis* polysaccharide; OBPP, oxidized BPP; *O*-CMCS, *O*-carboxymethyl chitosan. (b) Infrared spectra of BPP, OBPP, and OBPP/CMCS hydrogel. (c) Frequency sweep tests of OBPP/CMCS. (d) Strain sweep tests of OBPP/CMCS. (e) SEM images of OBPP/CMCS hydrogel. (f) Particle size distribution statistics of OBPP/CMCS. (g) Swelling ratio of OBPP/CMCS hydrogel. (h) In vitro wet mass retention profile of the OBPP/CMCS hydrogel. (i) Water loss rate of OBPP/CMCS hydrogel.

In summary, the optimal extraction conditions determined from single-factor experiments were as follows: temperature, 100 °C; extraction time, 55−65 min; liquid-to-solid ratio, 15:1−25:1 mL/g; and extraction cycles, 1−3.

3.2. Box-Behnken Design and Analysis

Experimental design and results were shown in Table S1. Regression analysis (Design Expert 8.0.6) yielded a second-order polynomial model: $Y = 7.42 + 0.041A + 0.39B + 1.11C - 0.86AB + 0.26AC + 0.63BC - 0.50A^2 - 0.75B^2 - 2.30C.^2$

The analysis of variance (ANOVA) results for the response surface methodology are summarized in Table 1. The model was found to be highly significant, with an *F*-value of 118.2 ($p < 0.0001$), while the lack-of-fit term was nonsignificant ($p = 0.9015$), confirming the adequacy and robustness of the model. The coefficient of determination (R^2) was 0.9935, indicating

https://doi.org/10.1021/acsomega.5c12446
ACS Omega 2026, 11, 20646−20656

excellent agreement between the predicted and experimental data. Moreover, the close correspondence between the adjusted R^2 (0.9851) and the predicted R^2 (0.9783), with a difference of less than 0.2, further supports the model's strong reliability and predictive accuracy. Among the evaluated factors, the p-value for factor A exceeded 0.05, suggesting that extraction time within the range of 55−65 min exerted minimal influence on polysaccharide yield, whereas the remaining factors had significant effects on extraction efficiency.

The three-dimensional response surface generated from the regression model is illustrated in Figure 1b. The response plots display steep gradients and tightly packed elliptical contour lines, suggesting strong interactive effects among the extraction parameters on BPP yield.[36] As evident from Figure 1b, the interaction between extraction time and extraction cycles, as well as between the number of cycles and the liquid-to-solid ratio, exhibited the most pronounced influence, findings that are consistent with the ANOVA results summarized in Table 1.

The optimized extraction parameters predicted by the model were an extraction time of 57.83 min, a liquid-to-solid ratio of 23.18 mL/g, and 2.30 extraction cycles. Considering practical experimental conditions, these parameters were adjusted to 58 min, 23 mL/g, and 2 extraction cycles, respectively. Validation experiments conducted in triplicate under these optimized conditions yielded an average BPP extraction efficiency of 7.49%, which closely matched the model's predicted value of 7.70%, confirming the reliability and predictive accuracy of the optimization model.

3.3. In Vitro Antioxidant Activity Assay

As shown in Figure 1c, BPP exhibited a clear concentration-dependent scavenging effect on all three free radicals within the concentration range of 0.2−4 mg/mL. The IC_{50} values for DPPH, hydroxyl, and $ABTS^+$ radical scavenging were determined to be 3.111, 1.540, and 1.024 mg/mL, respectively. Remarkably, complete (100%) scavenging of $ABTS^+$ radicals was achieved at a concentration of 4 mg/mL. These findings highlight the strong antioxidant capacity of BPP and underscore its potential as a natural and effective free radical scavenger.

The antioxidant capacity of BPP is consistent with the reported bioactivity of certain plant polysaccharides, which can act as antioxidants by donating hydrogen atoms from hydroxyl groups.[37] The observed concentration-dependent radical scavenging supports this hydrogen-donation mechanism. This property was leveraged by incorporating oxidized BPP into the OBPP/CMCS hydrogel. Although direct in vivo ROS scavenging remains to be validated, the established chemical antioxidant activity of BPP provides an experimental basis for its further application in wound dressing development.

3.4. Fourier Transform Infrared Analysis

BPP was oxidized with sodium periodate to generate aldehyde groups, yielding oxidized BPP. The OBPP then formed a cross-linked network via a Schiff base reaction with CMCS, as shown in Figure 2a. FT-IR spectroscopy was employed to elucidate the structural features of BPP, OBPP, and the OBPP/CMCS hydrogel. As shown in Figure 2b, BPP exhibited a broad and intense absorption band at 3436 cm^{-1}, corresponding to the stretching vibration of hydroxyl (−OH) groups. Following oxidation, the intensity of this peak decreased significantly, indicating a reduction in hydroxyl group content and partial disruption of the intermolecular hydrogen-bonding network. Moreover, the appearance of a characteristic absorption band at 1740 cm^{-1}, characteristic of the C═O stretching vibration, confirmed the successful oxidation of BPP.[38]

In the OBPP/CMCS hydrogel, the C═O stretching band at 1737 cm^{-1} became significantly weaker, while the band at 1606 cm^{-1} intensified and broadened, suggesting the formation of new C═N bonds. This shift is indicative of a Schiff base reaction between the amino groups of CMCS and the aldehyde groups of OBPP, confirming successful cross-linking within the hydrogel matrix.

The aldehyde content of oxidized OBPP was quantitatively determined using the hydroxylamine hydrochloride titration method and calculated to be 4.46 ± 0.09 mmol/g. To further assess the biosafety of the hydrogel system, residual free aldehyde groups in the hydrogel supernatant were also measured using the same method. No detectable aldehyde signal was observed, indicating that the aldehyde groups were almost completely consumed during the cross-linking and subsequent purification process.

3.5. Rheology Analysis

The rheological behavior of the OBPP/CMCS hydrogel is illustrated in Figure 2c. At angular frequencies of 1, 10, and 100 $rad{\cdot}s^{-1}$, the G' values (7.50 ± 0.17, 7.49 ± 0.20, and 15.17 ± 4.68 Pa, respectively) were consistently higher than the G'' values (0.96 ± 0.18, 0.95 ± 0.15, and 1.89 ± 0.05 Pa, respectively). The storage modulus (G'), representing the elastic or solid-like characteristics of the material, consistently exceeded the loss modulus (G''), which reflects the viscous or liquid-like response. This dominance of G' over G'' confirms the formation of a well-developed gel network with pronounced elastic behavior. Furthermore, the minimal frequency dependence of both moduli suggests a stable and highly cross-linked hydrogel structure with strong internal cohesion and mechanical integrity. The amplitude sweep results are presented in Figure 2d. The linear viscoelastic region of the hydrogel spanned from 1% to 10.3% shear strain, with a yield point observed at approximately 440% shear strain, indicating the excellent mechanical resilience of the OBPP/CMCS hydrogel.

3.6. Scanning Electron Microscopy Analysis

The SEM micrographs of the OBPP/CMCS hydrogel (Figure 2e) reveal a highly porous and well-interconnected three-dimensional architecture. Such a network not only characterizes the morphology but also provides an extensive surface area conducive to cell attachment, nutrient diffusion, and tissue infiltration. The pore size of the hydrogel was quantified using ImageJ software. SEM images were acquired at ×100 magnification (3 images, 10 fields of view per image). Thresholding and segmentation were performed automatically in ImageJ with minor manual correction to ensure accurate identification of pore boundaries. As shown in Figure 2f, quantitative analysis revealed a mean pore size of 55.22 ± 2.89 μm. This porous architecture is conducive to wound exudate uptake, gas exchange, and the diffusion of nutrients and bioactive substances. Moreover, the lamellar and wrinkled nature of the pore walls substantially increases the hydrogel's specific surface area, enhancing its water retention capacity. This structural configuration minimizes adhesion between the dressing and newly formed granulation tissue during dressing changes, reducing the risk of secondary injury. The resulting moist and protected wound environment promotes epithelial cell migration and proliferation, ultimately facilitating rapid re-epithelialization and tissue regeneration.

https://doi.org/10.1021/acsomega.5c12446
ACS Omega 2026, 11, 20646−20656

3.7. Swelling Index and Water Loss Rate

The swelling behavior and water retention properties of the hydrogel were assessed at 37 °C. Swelling capacity is a critical parameter for determining a hydrogel's ability to absorb fluid and sustain a moist wound environment. An ideal wound dressing should exhibit high absorbency to efficiently uptake wound exudate and facilitate the healing process.[39]

As illustrated in Figure 2g, the swelling ratio increased rapidly within the first 4 h at both 5.5 and 7.4 pH values, suggesting that water molecules could readily penetrate the hydrogel's three-dimensional polymeric network. This behavior reflects the hydrogel's prompt responsiveness and strong water absorption capacity under physiological conditions. With time, the swelling rate gradually declined until equilibrium was achieved. The subsequent slower swelling phase maintains prolonged hydration, providing sustained moisture and protection to the wound surface. After reaching swelling equilibrium, the long-term stability of the hydrogel was evaluated by monitoring its mass retention over time. As shown in Figure 2h, the hydrogel exhibited a pH-dependent stability profile, undergoing a much faster wet mass loss at pH 5.5 than at pH 7.4, which is ascribed to the hydrolysis of its acid-labile imine cross-links.[40−42] The stability profiles under both pH conditions conformed to first-order kinetics throughout the 120 h study period. At pH 5.5, linear fitting yielded ln $(W_a/W_0) = -0.0217$ t ($R^2 = 0.96$), corresponding to a degradation rate constant $k = 0.52$ day $^{-1}$. At pH 7.4, the fitting equation was ln $(W_a/W_0) = -0.0071$ t ($R^2 = 0.99$), corresponding to $k = 0.17$ day $^{-1}$. The degradation rate at pH 5.5 was 3.1-fold higher than that at pH 7.4. After 120 h, only 7.1% of the initial mass remained at pH 5.5, compared to 30.9% at pH 7.4, demonstrating that the acidic condition induced near-complete structural disintegration of the hydrogel network. Clinical studies have shown that wound pH is not static during healing; it is typically alkaline in the initial phase and gradually decreases toward neutrality as healing progresses.[43] In chronic or infected wounds, bacterial metabolism and inflammatory cell activity can create localized acidic microenvironments. Under normal physiological conditions, the hydrogel maintains structural integrity, serving as a stable wound barrier. In acidic microenvironments, accelerated degradation could facilitate timely dressing removal or localized release of bioactive components, potentially reducing mechanical trauma to regenerating tissue.

A moist wound environment is essential for tissue regeneration, as it promotes epithelial cell migration and re-epithelialization. Therefore, the water retention ability of the OBPP/CMCS hydrogel was further investigated through water evaporation tests. As shown in Figure 2i, the hydrogel exhibited excellent water retention, with a 12 h water loss rate of only 27.74%, demonstrating its strong capacity to preserve moisture and highlighting its potential utility as an effective wound dressing material.[13,39]

3.8. Hydrolysis and Cell Viability Assay

The cytocompatibility of BPP and OBPP/CMCS hydrogel extracts was assessed using the CCK-8 assay, as illustrated in Figure 3a,b. Across all tested concentrations (50−800 μg/mL), neither the BPP solution nor the hydrogel extracts induced cytotoxicity, confirming their excellent biocompatibility. This performance was higher than the cell viability (92%) reported for pure CMC films.[44] Higher concentrations of both BPP and the OBPP/CMCS hydrogel extracts significantly enhanced HUVEC proliferation in a dose-dependent manner. Further studies are necessary to elucidate the underlying mechanisms and identify the specific chemical features responsible for this pro-proliferative effect.

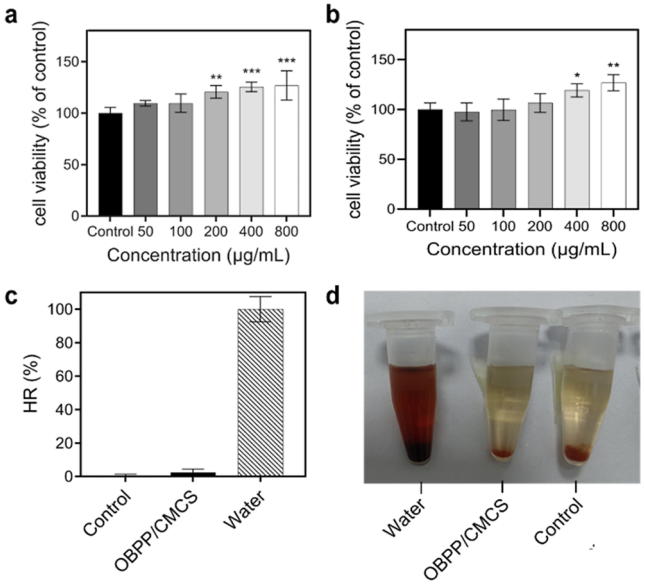

Figure 3. In vitro biocompatibility evaluation of BPP and OBPP/CMCS hydrogel. (a) Effect of BPP on HUVECs viability. (b) Effects of OBPP/CMCS hydrogel on HUVECs viability (*$p < 0.05$, **$p < 0.01$, ***$p < 0.001$, vs Control). (c) The quantitative analysis of the hemolytic activity of OBPP/CMCS hydrogel. (d) The image of the hemolytic activity of OBPP/CMCS hydrogel.

The hemocompatibility of the OBPP/CMCS hydrogel was further evaluated, as shown in Figure 3c,d. Red blood cells exposed to distilled water underwent complete hemolysis, producing a red supernatant, whereas those treated with physiological saline or the hydrogel extract remained intact, resulting in a nearly colorless supernatant. The measured hemolysis ratio (HR %) of 2.46% was substantially below the permissible limit of 5% for biomedical materials, confirming the outstanding blood compatibility of the OBPP/CMCS hydrogel.

3.9. In Vitro Wound Healing

HUVECs were used as a common model to assess pro-angiogenic activity, a critical process in wound healing. Their relevance is supported by studies showing HUVEC-derived matrices can promote skin cell adhesion and that their migration is a key target for bioactive wound dressings.[45−47] The migratory response of HUVECs to BPP and OBPP/CMCS hydrogel extracts was investigated using the cell scratch assay, as depicted in Figure 4. Following scratch induction, cellular migration was monitored at 24 and 48 h, and the wound closure rate was quantified using ImageJ software. As illustrated in Figure 4a,b, after 48 h of incubation, BPP exhibited a modest enhancement in cell migration, with statistically significant improvement observed only at 400 μg/mL. However, the OBPP/CMCS hydrogel significantly promoted HUVEC migration, demonstrating pronounced wound closure at both 400 and 800 μg/mL. These findings, supported by quantitative analysis in Figure 4c,d, indicate that the OBPP/CMCS hydrogel possesses pro-migratory potential, which may contribute to its wound-healing efficacy. These effects were observed using hydrogel extracts, suggesting that soluble factors released from the matrix contribute to its bioactivity. This pro-migratory effect suggests that the OBPP/CMCS hydrogel shares a similar functional goal

https://doi.org/10.1021/acsomega.5c12446
ACS Omega 2026, 11, 20646−20656

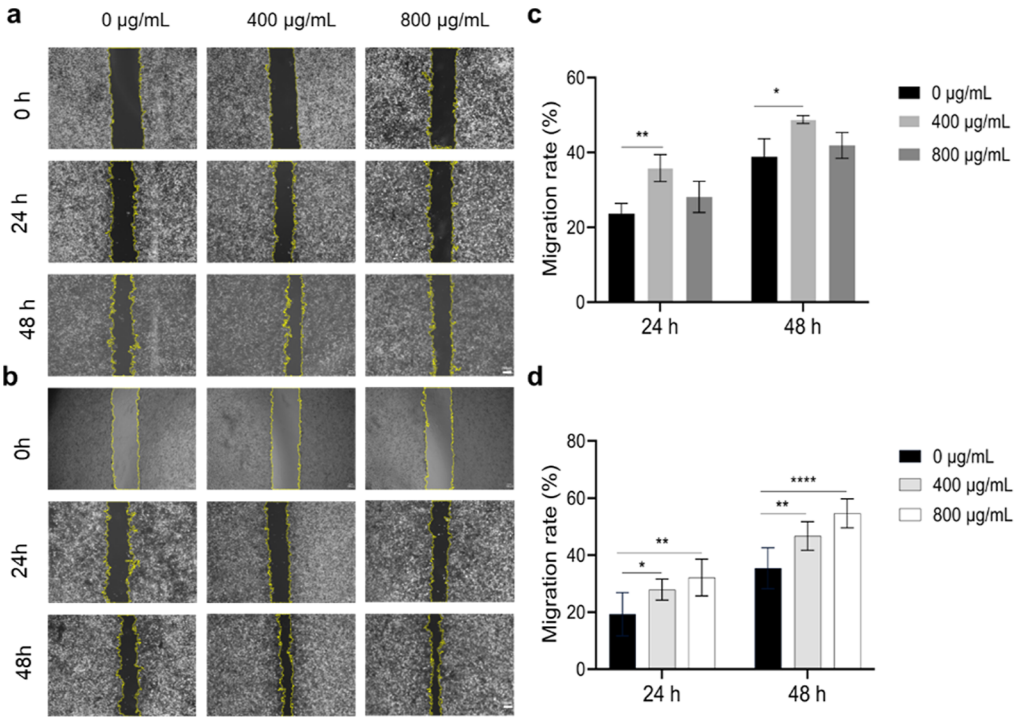

Figure 4. Cell migration ability of BPP and OBPP/CMCS hydrogel. (a) The migration images of HUVECs incubated with BPP for 0, 24, and 48 h. (b) The migration images of HUVECs incubated with OBPP/CMCS hydrogel for 0, 24, and 48 h. (c) Cell migration rate of BPP. (d) Cell migration rate of OBPP/CMCS hydrogel (*$p < 0.05$, **$p < 0.01$, ***$p < 0.001$, vs Control).

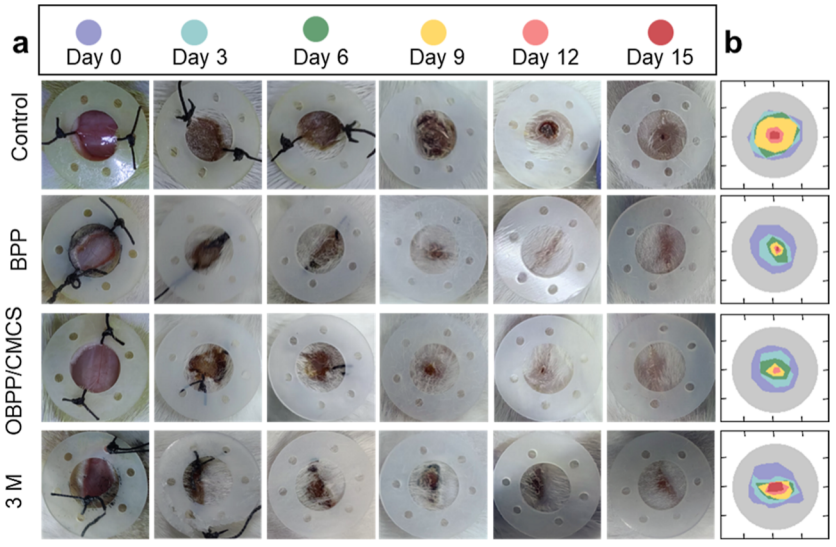

Figure 5. Wound healing effects of OBPP/CMCS in mice. (a) Representative images of wound healing. (b) Quantification of Wound Closure.

with advanced strategies designed to promote wound angiogenesis, such as dressings incorporating synthetic VEGF-mimetic peptides.[47] Importantly, achieving this bioactivity with a more accessible and simplified plant polysaccharide system underscores the application potential of the OBPP/CMCS hydrogel as a novel class of wound dressing.

3.10. In Vivo Wound Healing

To assess the wound healing efficacy of the prepared hydrogel as a potential wound dressing, full-thickness excisional wounds were established on the dorsal surface of mice. Wound healing was then monitored by tracking wound area reduction and by histological analysis. The macroscopic healing process following treatment with BPP solution, OBPP/CMCS hydrogel, or commercial 3 M spray was monitored and is illustrated in Figure 5a. As shown in Figure 5b, both the polysaccharide and hydrogel-treated groups exhibited a significantly accelerated healing rate compared to the control group from day 3 onward. Quantitative analysis (Figure 6) revealed that on day 3, the residual wound area in the hydrogel group was significantly smaller (49.34 ± 2.43) % than that in the 3 M group (70.27 ± 13.20) % and the control group (72.45 ± 4.47) %. By day 9, this difference became more pronounced, with the hydrogel group achieving a residual wound area of only (7.59 ± 1.83) %, compared to (32.16 ± 6.12) % in the 3 M group and (44.14 ± 18.22) % in the control group. For comparison, a recently

https://doi.org/10.1021/acsomega.5c12446
ACS Omega 2026, 11, 20646−20656

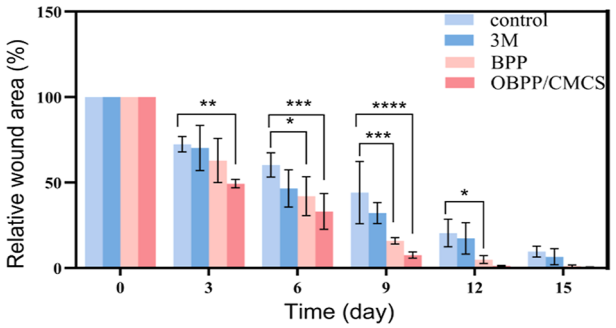

Figure 6. Comparison of remaining wound area percentage to initial wound area between control group, BPP group, OBPP/CMCS group, and 3 M group (*$p < 0.05$, **$p < 0.01$, ***$p < 0.001$, ****$p < 0.0001$ vs Control).

reported Konjac glucomannan/*Bletilla striata* polysaccharide composite hydrogel showed a residual wound area of (5.45 ± 0.45) % by day 10 in a similar murine model, with the corresponding control group exhibiting (16.77 ± 1.1) % residual area.[48] These results confirm the efficacy of the OBPP/CMCS hydrogel in promoting rapid wound closure. By day 15, the wound area in the hydrogel-treated group had nearly completely closed (0.41 ± 0.28) %, whereas the 3 M group (6.59 ± 4.68) % and control group (9.63 ± 3.20) % still showed incomplete closure. Besides, the hydrogel group exhibited the most advanced wound healing, characterized by light pink skin coloration, a smooth wound surface, and an absence of scabbing. The other treatment groups showed incomplete closure or persistent scab formation.

Histological examination of wound tissues on day 15, as shown in Figure 7, further substantiated these macroscopic observations. Relative to normal skin, the OBPP/CMCS hydrogel group demonstrated the most favorable tissue regeneration profile. The epidermis appeared continuous and uniform in thickness, closely resembling that of normal skin (black arrows). Collagen fibers were densely and orderly arranged (red arrows), and newly formed skin appendages were evident (green arrows), indicating advanced tissue remodeling. The BPP-treated group also showed nearly complete epidermal restoration with moderately aligned collagen fibers and a limited number of skin appendages, suggestive of partial repair. The blank control group exhibited pronounced epidermal hyperplasia in the granular and spinous layers, disorganized collagen architecture, and an absence of appendages or hair follicles, indicative of delayed healing. The 3 M commercial dressing group displayed epidermal thickening, inflammatory cell infiltration (purple arrows), and a lack of skin appendages, signifying inferior repair efficiency. These findings confirm that the OBPP/CMCS hydrogel significantly accelerates wound closure and improves tissue regeneration, primarily by promoting collagen alignment, re-epithelialization, and hair follicle neogenesis, key features of effective wound healing.

The in vivo results confirm the pro-healing efficacy of the OBPP/CMCS hydrogel in a mouse model of acute full-thickness skin defect. However, it is important to recognize that this classic model differs from clinical chronic infected wounds which are frequently characterized by complex microbial infections. Despite this limitation, the present findings establish an important foundation for the application of this material system. Future studies may further investigate its efficacy in more complex wound models, such as diabetic ulcers.

4. CONCLUSIONS

This study successfully extracted and optimized the preparation process of the bioactive polysaccharide BPP from the natural plant *B. paridiformis*. The extracted polysaccharides demonstrated remarkable antioxidant capacity and significant cell proliferation-promoting activity. Building upon these findings, an oxidation-based modification strategy was developed to convert BPP into an oxidized derivative, which was subsequently incorporated into a CMCS matrix to construct a hydrogel system for wound management. Comprehensive physicochemical characterization revealed that the resulting OBPP/CMCS hydrogel possessed a highly porous three-dimensional network, excellent swelling behavior, and superior water retention capacity, attributes that together create an optimal moist microenvironment conducive to tissue repair. In vitro assays confirmed the outstanding cytocompatibility of the hydrogel and its ability to promote cellular proliferation and migration, while in vivo studies demonstrated significantly accelerated wound closure and improved tissue regeneration, accompanied by reduced scar formation and restoration of skin appendages. In summary, this study provides experimental evidence for the development of functional wound dressings based on natural polysaccharides.

In parallel, this study identifies clear directions for future research. Further purification and structural elucidation of BPP will enable a deeper understanding of its physicochemical and biological properties, establish clearer structure−property relationships, and allow precise control over its functionalization and cross-linking behavior. Several important functionalities of the hydrogel system as a wound dressing, such as its antimicrobial activity and immunomodulatory effects on the wound microenvironment, require systematic evaluation. The deeper molecular mechanisms by which it promotes tissue regeneration require further investigation. Furthermore, functionalization strategies such as including drug loading, incorporation of active factors, or the design of stimulus-responsive systems could be employed to develop more targeted delivery and therapeutic platforms, addressing the treatment needs of complex chronic wounds such as diabetic ulcers. These directions establish a defined pathway for subsequent research.

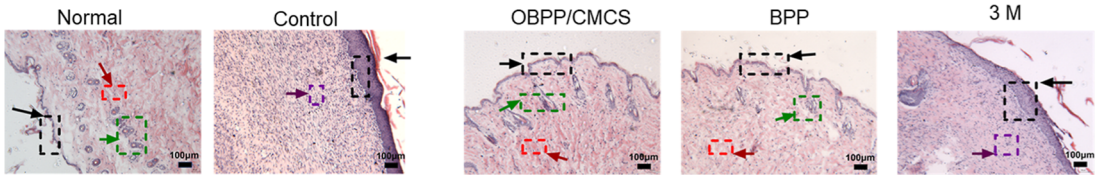

Figure 7. H & E staining of skin tissue in each treatment group.

https://doi.org/10.1021/acsomega.5c12446
ACS Omega 2026, 11, 20646−20656

■ ASSOCIATED CONTENT

Supporting Information

The Supporting Information is available free of charge at https://pubs.acs.org/doi/10.1021/acsomega.5c12446.

This Supporting Information provides details on the experimental methods for BPP extraction, optimization, and antioxidant activity assays (PDF)

■ AUTHOR INFORMATION

Corresponding Authors

Sitong Wu − *Shenyang Key Laboratory of Medical Molecular Theranostic Probes in School of Pharmacy, Shenyang Medical College, Shenyang 110034, China;* orcid.org/0009-0005-5255-3939; Email: wusitong@symc.edu.cn

Qing Chen − *Shenyang Key Laboratory of Medical Molecular Theranostic Probes in School of Pharmacy, Shenyang Medical College, Shenyang 110034, China*; Email: chenqing0906@symc.edu.cn

Xifan Mei − *School of Basic Medicine, Shenyang Medical College, Shenyang 110034, China;* orcid.org/0000-0003-3698-0525; Email: meixifan@jzmu.edu.cn

Authors

Na Zou − *School of Basic Medicine, Shenyang Medical College, Shenyang 110034, China*

Jie Zhou − *Shenyang Key Laboratory of Medical Molecular Theranostic Probes in School of Pharmacy, Shenyang Medical College, Shenyang 110034, China*

Complete contact information is available at: https://pubs.acs.org/10.1021/acsomega.5c12446

Author Contributions

§N.Z. and J.Z. made equal contributions to this work. N.Z.: Investigation, Validation, Data curation, Formal analysis, Visualization, Writing—original draft. J.Z.: Investigation, Visualization, Formal analysis, Validation, Writing—original draft. X.M.: Funding acquisition, Supervision, Validation, Writing—review and editing. Q.C.: Funding acquisition, Supervision, Formal analysis, Writing—review and editing. S.W.: Project administration, Conceptualization, Software, Methodology, Formal analysis, Writing—original draft, review and editing, Funding acquisition.

Notes

Ethics ApprovalThe research protocol was approved by the Animal Experiment Ethics Committee of Shenyang Medical University of TCM (Approval: SYYXY2024120201).
The authors declare no competing financial interest.

■ ACKNOWLEDGMENTS

This work was supported by the Natural Science Foundation of Liaoning Province (Grant No. 2023-BSBA-293), Shenyang Medical College Postgraduate Science and Technology Innovation Fund Program (Grant No. Y20250508), the Future Industry Frontier Technology Project of the Liaoning Provincial Department of Science and Technology (Grant No. 2025080219-JH2/1013), the Self-Developed Research Project of the Education Department of Liaoning Province (Grant No. JYTMS20231407), the Shenyang Young and Middle-aged Science and Technology Innovation Talent Project (Grant No. RC230168), the Liaoning Province Key Laboratory for Phenomics of Human Ethnic Specificity and Critical Illness (Grant No. [2022]59), and the National Undergraduate Training Program on Innovation and Entrepreneurship (Grant No. 20259017).

■ REFERENCES

(1) Dai, C.; Shih, S.; Khachemoune, A. Skin Substitutes for Acute and Chronic Wound Healing: An Updated Review. *J. Dermatol. Treat.* **2020**, *31*, 639−648.

(2) Peña, O. A.; Martin, P. Cellular and Molecular Mechanisms of Skin Wound Healing. *Nat. Rev. Mol. Cell Biol.* **2024**, *25*, 599−616.

(3) Yang, D.; Chen, H. L.; Wei, H.; Liu, A.; Wei, X. D.; Chen, J. Hydrogel Wound Dressings Containing Bioactive Compounds Originated from Traditional Chinese Herbs: A Review. *Smart Mater. Med.* **2024**, *5*, 153−165.

(4) Ding, X.; Tang, Q.; Xu, Z.; Xu, Y.; Zhang, H.; Zheng, D.; Wang, S.; Tan, Q.; Maitz, J.; Maitz, P. K.; et al. Challenges and Innovations in Treating Chronic and Acute Wound Infections: From Basic Science to Clinical Practice. *Burns Trauma* **2022**, *10*, tkac014.

(5) Liang, Y. P.; He, J. H.; Guo, B. L. Functional Hydrogels as Wound Dressing to Enhance Wound Healing. *ACS Nano* **2021**, *15*, 12687−12722.

(6) Wang, T.; Yi, W. W.; Zhang, Y.; Wu, H.; Fan, H. W.; Zhao, J. L.; Wang, S. Sodium Alginate Hydrogel Containing Platelet-Rich Plasma for Wound Healing. *Colloids Surf., B* **2023**, *222*, 113096.

(7) Stanciu, M. C.; Teacă, C. A. Natural Polysaccharide-Based Hydrogels Used for Dye Removal. *Gels* **2024**, *10*, 243.

(8) Deng, Z. H.; Yang, Z. L.; Yi, S.; Liu, Z. Q. Hydrogel-Exosome Systems in the Treatment of Refractory Diabetic Ulcers: Mechanisms, Progress, and Prospects. *Eur. Cells Mater.* **2025**, *53*, 82−97.

(9) Zhang, W.; Liu, L.; Cheng, H.; Zhu, J.; Li, X.; Ye, S.; et al. Hydrogel-Based Dressings Designed to Facilitate Wound Healing. *Mater. Adv.* **2024**, *5*, 1364−1394.

(10) Bei, Z.; Ye, L.; Tong, Q.; Ming, Y.; Yang, T.; Zhu, Y.; Zhang, L.; Li, X.; Deng, H.; Liu, J.; et al. Thermostimulated Shrinking and Adhesive Hydrogel Dressing for Treating Chronic Diabetic Wounds. *Cell Rep. Phys. Sci.* **2024**, *5*, 102289.

(11) Zhang, C.; Niu, J.; Li, J.; Zhang, H.; Yu, Q. L.; Chen, Y.; et al. Polysaccharide Based Supramolecular Injectable Hydrogels for in Situ Treatment of Bladder Cancer. *Chin. Chem. Lett.* **2024**, *35*, 108556.

(12) Venkatesan, J. K.; Liu, W.; Madry, H.; Cucchiarini, M. Alginate Hydrogel-Guided RAAV-Mediated FGF-2 and TGF-β Delivery and Overexpression Stimulates the Biological Activities of Human Meniscal Fibrochondrocytes for Meniscus Repair. *Eur. Cells Mater.* **2024**, *47*, 1−14.

(13) Chen, X.; Hu, Z.; Zhao, K.; Rao, X.; Shen, C.; Chen, Y.; Ye, X.; Fang, C.; Zhou, F.; Ding, Z.; et al. Microenvironment-Responsive, Multimodulated Herbal Polysaccharide Hydrogel for Diabetic Foot Ulcer Healing. *Sci. Rep.* **2024**, *14*, 22135.

(14) Gong, H.; Li, W.; Sun, J.; Jia, L.; Guan, Q.; Guo, Y.; Wang, Y. A Review on Plant Polysaccharide Based on Drug Delivery System for Construction and Application, with Emphasis on Traditional Chinese Medicine Polysaccharide. *Int. J. Biol. Macromol.* **2022**, *211*, 711−728.

(15) Manzoor, A.; Dar, A. H.; Pandey, V. K.; Shams, R.; Khan, S.; Panesar, P. S.; et al. Recent Insights into Polysaccharide-Based Hydrogels and Their Potential Applications in Food Sector: A Review. *Int. J. Biol. Macromol.* **2022**, *213*, 987−1006.

(16) Xu, B.; Li, S.; Ding, W.; Zhang, C.; Rehman, M. U.; Tareen, M. F.; et al. From Structure to Function: A Comprehensive Overview of Polysaccharide Roles and Applications. *Food Front* **2025**, *6*, 15−39.

(17) Guan, Y. M.; Cheng, H. T.; Zhang, L. L.; Zhang, Y.; Pan, X. X.; Jin, Q.; et al. Anthracnose of *Brachybotrys paridiformis* Caused by *Colletotrichum siamense* in Northeast China. *Plant Dis.* **2024**, *108*, 794.

(18) Zhou, B. S. *Chemical Constituents, Anti Ulcerative Colitis Activity and Pharmacokinetics of Brachybotrys paridiformis Maxim. ex Oliv*; Jilin University, 2022.

(19) Wu, S. T.; Wang, Y. X.; Yu, B. H.; Ma, C. L.; Qiu, H. Q.; Wang, G. S. Phenylpropanoids from *Brachybotrys paridiformis* Maxim. ex Oliv. and Their Anti-HBV Activities. *Phytochemistry* **2022**, *197*, 113114.
(20) Wu, S. T.; Li, F.; Wang, Y. X.; Yu, B. H.; Ma, C. L.; Qiu, H. Q.; et al. Phenylpropanoids from *Brachybotrys paridiformis* Maxim. ex Oliv. and Their Anti-HBV Activities (II). *Phytochemistry* **2022**, *203*, 113364.
(21) Yan, Y.; Guan, S.; Wang, S.; Xu, J.; Sun, C. Synthesis and Characterization of Protocatechuic Acid Grafted Carboxymethyl Chitosan with Oxidized Sodium Alginate Hydrogel through the Schiff's Base Reaction. *Int. J. Biol. Macromol.* **2022**, *222*, 2581−2593.
(22) Kruczkowska, W.; Kłosiński, K. K.; Grabowska, K.; Gałęziewska, J.; Gromek, P.; Kciuk, M.; Kałuzińska-Kołat, Ż.; Kołat, D.; Wach, R. A. Medical Applications and Cellular Mechanisms of Action of Carboxymethyl Chitosan Hydrogels. *Molecules* **2024**, *29*, 4360.
(23) Peng, Y.; Zhang, J.; Yang, H.; Yang, Z.; Xue, H.; Wu, F.; et al. Acetylation Modification and Antioxidant Activity of Polysaccharides from *Agrocybe cylindracea*. *J. Food Meas. Charact.* **2022**, *16*, 1911−1919.
(24) Li, R. L.; Zhou, J. N.; Zhang, X. Y.; Zhang, T.; Wang, J.; Zhang, M.; He, C.; Chen, H. Isolation, Structural Characterization and Cholesterol-Lowering Effects of a Novel Polysaccharide from Mulberry (*Morus alba* L.) Leaf. *Ind. Crops Prod.* **2023**, *202*, 117010.
(25) Ahmad, M. M. Characterization and Antioxidant Activities of Polysaccharides Extracted from Flageolet Bean Pods Waste. *Curr. Res. Green Sustainable Chem.* **2021**, *4*, 100154.
(26) Zhang, H.; Zou, P.; Zhao, H.; Qiu, J.; Regenstein, J. M.; Yang, X. Isolation, Purification, Structure and Antioxidant Activity of Polysaccharide from Pinecones of *Pinus koraiensis*. *Carbohydr. Polym.* **2021**, *251*, 117078.
(27) Thambiraj, S. R.; Phillips, M.; Koyyalamudi, S. R.; Reddy, N. Yellow Lupin (*Lupinus luteus* L.) Polysaccharides: Antioxidant, Immunomodulatory and Prebiotic Activities and Their Structural Characterisation. *Food Chem.* **2018**, *267*, 319−328.
(28) Li, F.; Liu, T. T.; Liu, X.; Han, C. Y.; Li, L. L.; Zhang, Q.; Sui, X. *Ganoderma lucidum* polysaccharide hydrogel accelerates diabetic wound healing by regulating macrophage polarization. *Int. J. Biol. Macromol.* **2024**, *260* (Pt 2), 129682.
(29) Zhang, H.; Wang, K.; Zhang, Y.; Cui, Y. L.; Wang, Q.; Li, Q.; et al. A Self-Healing Hydrogel Wound Dressing Based on Oxidized *Bletilla striata* Polysaccharide and Cationic Gelatin for Skin Trauma Treatment. *Int. J. Biol. Macromol.* **2023**, *253*, 127189.
(30) Zhou, Z. Q.; Zhang, X. J.; Xu, L. J.; Lu, H. J.; Chen, Y. Y.; et al. A self-healing hydrogel based on crosslinked hyaluronic acid and chitosan to facilitate diabetic wound healing. *Int. J. Biol. Macromol.* **2022**, *220*, 326−336.
(31) Liu, J.; Qu, M.; Wang, C.; Xue, Y.; Huang, H.; Chen, Q.; Sun, W.; Zhou, X.; Xu, G.; Jiang, X. A Dual-Cross-Linked Hydrogel Patch for Promoting Diabetic Wound Healing. *Small* **2022**, *18*, 2106172.
(32) Zhang, X.; Zhao, M.; Cao, N.; Qin, W.; Zhao, M.; Wu, J.; et al. Construction of a Tumor Microenvironment pH-Responsive Cleavable PEGylated Hyaluronic Acid Nano-Drug Delivery System for Colorectal Cancer Treatment. *Biomater. Sci.* **2020**, *8*, 1885−1896.
(33) Yin, X.; Hao, Y.; Lu, Y.; Zhang, D.; Zhao, Y.; Mei, L.; Sui, K.; Zhou, Q.; Hu, J. Bio-Multifunctional Hydrogel Patches for Repairing Full-Thickness Abdominal Wall Defects. *Adv. Funct. Mater.* **2021**, *31*, 2105614.
(34) Yu, Y. F.; Yang, B.; Tian, D. L.; Liu, J.; Yu, A.; Wan, Y.; et al. Thiolated Hyaluronic Acid/Silk Fibroin Dual-Network Hydrogel Incorporated with Bioglass Nanoparticles for Wound Healing. *Carbohydr. Polym.* **2022**, *288*, 119334.
(35) Wei, X. X. E. *Isolation, Purification and Antioxidant Activity of Polysaccharides from Elderberry Fruit*; Shandong Agricultural University, 2023.
(36) Niu, L. L.; Wu, Y. R.; Liu, H. P.; Wang, Q.; Li, M. Y.; Jia, Q. Optimization of Extraction Process, Characterization and Antioxidant Activities of Polysaccharide from *Leucopaxillus giganteus*. *J. Food Meas. Charact.* **2021**, *15*, 2842−2853.
(37) Mu, S.; Yang, W. J.; Huang, G. L. Antioxidant activities and mechanisms of polysaccharides. *Chem. Biol. Drug Des* **2021**, *97* (3), 628−632.
(38) Yu, Z. J.; Li, Q.; He, X.; Wang, X. C.; Wen, Y.; Zeng, L. Y.; et al. A multifunctional hydrogel based on nature polysaccharide fabricated by Schiff base reaction. *Eur. Polym. J.* **2023**, *197*, 112330.
(39) Richbourg, N. R.; Wancura, M.; Gilchrist, A. E.; Toubbeh, S.; Harley, B. A. C.; Cosgriff-Hernandez, E.; Peppas, N. A. Precise Control of Synthetic Hydrogel Network Structure via Linear, Independent Synthesis-Swelling Relationships. *Sci. Adv.* **2021**, *7*, No. eabe3245.
(40) Zhang, Y. J.; Zhang, L.; Wu, P. L.; Wu, S.; Qin, J. H.; Zhang, H. S.; et al. pH- and glucose-responsive antioxidant hydrogel promotes diabetic wound healing. *Biomater Adv.* **2025**, *169*, 214177.
(41) Su, Y.; Xu, J.; Liu, W.; Shu, Y.; Ma, H. L.; Cheng, Y. Y.; et al. A gelatin/acrylamide-based hydrogel for smart drug release monitoring and radiation-induced wound repair in breast cancer. *Int. J. Biol. Macromol.* **2024**, *283*, 137845.
(42) Xie, H. L.; Tian, S. B.; Cui, C.; Sun, C. L.; Hu, Y.; Tang, C.; et al. A glycopeptide-based pH-responsive hydrogel promotes diabetic wound healing via antimicrobial and remodeling microenvironment. *Colloids Surf. B Biointerfaces* **2025**, *251*, 114614.
(43) Shukla, V. K.; Shukla, D.; Tiwary, S. K.; Agrawal, S.; Rastogi, A. Evaluation of pH measurement as a method of wound assessment. *J. Wound Care* **2007**, *16*, 291−294.
(44) Basu, P.; Narendrakumar, U.; Arunachalam, R.; Devi, S.; Manjubala, I. Characterization and Evaluation of Carboxymethyl Cellulose-Based Films for Healing of Full-Thickness Wounds in Normal and Diabetic Rats. *ACS Omega* **2018**, *3* (10), 12622−12632.
(45) Li, J. Y.; Zhai, D.; Lv, F.; Yu, Q. Q.; Ma, H.; Yin, J.; et al. Preparation of copper-containing bioactive glass/eggshell membrane nanocomposites for improving angiogenesis, antibacterial activity and wound healing. *Acta Biomater* **2016**, *36*, 254−266.
(46) Solomon, D. E. An in vitro examination of an extracellular matrix scaffold for use in wound healing. *Int. J. Exp Pathol* **2002**, *83* (5), 209−216.
(47) Chen, Z. J.; Wang, L. L.; Guo, C. J.; Qiu, M. L.; Cheng, L.; Chen, K. Z.; et al. Vascularized polypeptide hydrogel modulates macrophage polarization for wound healing. *Acta Biomater* **2023**, *155*, 218−234.
(48) Hao, Y.; Wang, J.; Zhang, H.; Liu, Q.; Wang, X.; Wei, Y.; et al. Konjac glucomannan/*Bletilla striata* polysaccharide composite hydrogel: A promising anti-inflammatory dressing for accelerated wound healing. *Carbohydr. Polym.* **2025**, *361*, 123639.

https://doi.org/10.1021/acsomega.5c12446
ACS Omega 2026, 11, 20646−20656